Three-Level Inverter-Based Shunt Active Power Filter in Three-Phase Three-Wire and Four-Wire Systems

Oleg Vodyakho, *Member, IEEE*, and Chris C. Mi, *Senior Member, IEEE*

***Abstract*—This paper presents a direct current-space-vector control of an active power filter (APF) based on a three-level neutral-point-clamped (NPC) voltage-source inverter. The proposed method indirectly generates the compensation current reference by using an equivalent conductance of the fundamental component using APF's dc-link voltage control. The proposed control can selectively choose harmonic current components by real-time fast Fourier transform to generate the compensation current. The compensation current is represented in a rotating coordinate system with chosen switching states from a switching table implemented in a field-programmable gate array. In addition, a three-phase four-wire APF based on a three-level neutral-point-clamped inverter is also presented. The proposed APF eliminates harmonics in all three phases as well as the neutral current. A three-phase three-wire NPC inverter system can be used as a three-phase four-wire system since the split dc capacitors provide a neutral connection. To regulate and balance the split dc-capacitor voltages, a new control method using a sign cubical hysteresis controller is proposed. The characteristics of the APF system with an *LCL*-ripple filter are investigated and compared with traditional current control strategies to evaluate the inherent advantages. The simulation and experimental results validated the feasibility of the proposed APF.**

***Index Terms*—Direct current control (DCC), multilevel inverters, neutral clamped, power factor correction, power filter, reactive power compensation, shunt active filter, space vector, three-phase four-wire system, voltage-source inverter (VSI).**

I. Introduction

A LARGE portion of the total electrical energy produced in the world supplies different types of nonlinear loads, such as variable-frequency drives and electronic ballasts. These loads are typically composed of odd harmonic currents, which are multiples of the fundamental frequency. The harmonic currents cannot contribute to active power and need to be eliminated to enhance power quality [1]. Active power filters (APFs) are designed for this purpose.

APFs in three-phase three-wire systems can be based on several control methods [2]–[9]. Typically, current control is performed either by pulsewidth modulation (PWM) [3], [4], [7] or by direct current control [9], [10]. For detection of undesired harmonic currents, closed-loop synchronous-frame regulators [4], [7] or integrating oscillators [3] can be implemented. However, these methods result in phase shifts, which reduce the filtering performance. A better approach is to use Fourier transformation to determine individual harmonics that need to be eliminated. The APF control proposed in this paper is based on the Fourier transformation approach.

Most APFs use a standard two-level voltage-source inverter (VSI) [6], [7]. However, for medium-voltage applications, three-level VSIs have been proven to be more advantageous [3], [8], [9]. A three-level neutral-point-clamped (NPC) inverter can be employed in three-phase three-wire systems, as well as three-phase four-wire systems [10], [11]. In a three-level NPC inverter, the splitting dc-capacitor voltage has to be maintained as half of the dc-link voltage.

The advantages of three-level VSIs include lower harmonic distortion, lower switching frequency, and lower power loss. APFs based on three-level inverters are generally more expensive but can be compensated by using smaller filter inductors, assuming the same switching frequency. However, the control of a three-level inverter is more complicated than a two-level inverter because of the large number of inverter switching states. Therefore, there is greater difficulty in synthesizing the voltage reference vector [12]. Typical current control strategy for the space vector PWM (SVPWM) control is based on stationary $\alpha\beta$-coordinates [12]. In this paper, a new current control, based on SV current control, is compared with the stationary $\alpha\beta$-coordinates based control. The proposed SV current controller (SVCC) [9] in the rotating coordinates uses five-level hysteresis CC (HCC), with sector selection strategy providing grid-voltage vector information, to decrease current ripple and number of switching. Although HCC-based SVCC for a three-level inverter has not been used for APF control, it is widely used in two-level VSI for motor drives [13].

The electric power distribution systems are inherently unbalanced due to untransposed distribution lines and unbalanced loads. Therefore, maintaining the distribution voltage within certain limits of a perfectly balanced waveform is very difficult. In addition, if the phases are unequally loaded, they produce undesired negative and zero-sequence currents. Under nonlinear voltage and current, the harmonic current will generate power losses. The negative sequence will cause excessive heating in machines and generate low-frequency ripples in rectifiers. The zero-sequence currents not only cause excessive power losses in neutral lines, but also degrade the circuit protection. For the neutral current (zero-sequence current) reduction, a zig–zag transformer is often employed, and the performance can be improved by using a zero-blocking transformer [14]. Unfortunately, this method has several disadvantages: 1) zero-sequence impedance of the zig–zag transformer must be low, thus requiring special design; 2) the effectiveness of the zig–zag transformer to

Manuscript received November 27, 2008; revised February 14, 2009. Current version published May 6, 2009. Recommended for publication by Associate Editor J. H. R. Enslin.

O. Vodyakho is with the Department of Electrical and Computer Engineering, Florida State University, Tallahassee, FL 32310 USA (e-mail: vodyakho@caps.fsu.edu).

C. C. Mi is with the Department of Electrical and Computer Engineering, University of Michigan, Dearborn, MI 48128 USA (e-mail: chrismi@umich.edu).

Digital Object Identifier 10.1109/TPEL.2009.2016663

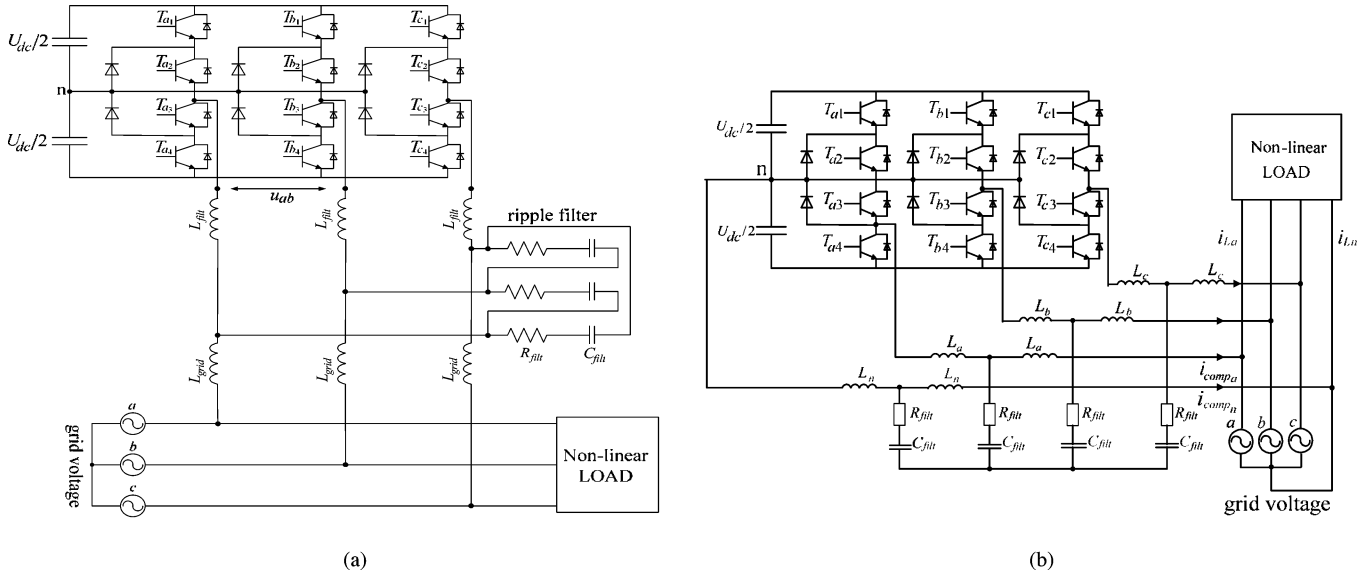

(a) (b)

Fig. 1. Three-level VSI-based APF in (a) three-phase three-wire systems, and (b) three-phase four-wire systems.

divert the third harmonic current is highly dependent on the distribution system impedance, and in most cases, only 50% reduction can be guaranteed; 3) a lower zero-sequence impedance increases the single-phase fault current level; therefore, fusing and circuit breaker resizing may be necessary; and 4) due to the reasons mentioned earlier, the passive zig–zag transformer approach is larger in size and weight. A better solution to reduce the neutral current is to utilize an APF in a four-wire system. Since a three-level VSI is used as an APF for a three-phase four-wire system, a strategy to balance the dc-link capacitor voltages is necessary [15]. This paper presents a new control strategy to balance the dc-link capacitor voltages by utilizing an opposite sign of the middle point current based on a three-level HCC [11].

The main focus of this paper is to study the performance of the SV current controls in a three-phase three-wire system with an *LCL* filter. The two SV current controls, one based on the stationary $\alpha\beta$- and the other on rotating *xy*-coordinates, are compared in order to analyze the influence of the *LCL* filter on the APF system in a three-phase three-wire system. In addition, the APF system in a four-wire system with and without an *LCL* filter is also analyzed.

II. Compensator Control Strategy

A. Calculation of APF Reference Current

An APF is considered as a controlled current source. Fig. 1 shows the configuration of an NPC three-level VSI for the application of an APF in three-phase three- and four-wire systems with an LCL-ripple filter. As illustrated in Fig. 1, the APF is connected in parallel with a nonlinear load to produce reactive and harmonic currents opposed to those of the nonlinear loads to cancel the harmonic currents.

It is assumed that the upper-leg and lower-leg capacitor voltages are identical, which is $U_{\rm dc}/2$. In the proposed control method, harmonics are decomposed by FFT. The FFT algorithm core implemented in the proposed APF uses the Cooley–Tukey algorithm [16] for digital computations. Nonsinusoidal periodical waves are analyzed to extract the fundamental component from the harmonics. The resultant FFT computations yield the amplitude and frequency of each harmonic component. Then, each harmonic is multiplied by the compensation factor. Therefore, only critical harmonics can be compensated and an APF does not need to cover all harmonic power.

The synchronous-reference-frame-based method has been widely used for most of the recent APFs. Synchronous fundamental *xy*-frame is derived from the SV transformation of the *abc*-coordinates. The detection of the harmonics is based on removing the dc-signal using a high-pass filter [7]. The synchronous harmonic *xy*-frame is similar to the fundamental *xy*-frame in principle. One difference is that the harmonic *xy*-coordinate frame rotates with a frequency the same as the selected harmonic. Thus, in the harmonic *xy*-frame, only the specific harmonic will be a dc-signal and all other frequencies including the fundamental will be ac-components [7]. One of the practical problems for this method is the implementation of the filters because of the software complexity. Those two methods require additional coordinate transformation from *xy*- to *abc*-coordinates for the PWM strategy.

The basic structure of the compensation in a three-wire system is based on the method described in [8]. The strategy based on the $\alpha\beta$-coordinates avoids instability problem in the case of regeneration. As illustrated in Fig. 2(a), the measured grid voltages ($\vec{e}_{\mathrm{grid}_{abc}}$) and load currents ($\vec{i}_{\mathrm{LOAD}_{abc}}$) are inputs of the FFT algorithm to extract only fundamental component (for grid voltages) and to select undesired harmonic current (for the load currents to provide flexibility to eliminate selected harmonics). The fundamental component of the grid voltage ($\vec{e}_{\mathrm{grid}(1)_{abc}}$) is extracted by the FFT for the disturbance-free identification/measurement. The fundamental grid voltages are transformed to $\alpha\beta$-coordinates ($\vec{e}_{\mathrm{grid}(1)\alpha\beta}$) and the position of the grid-voltage vector is identified (γ) to be used for the sector selection. The dc-voltage controller output signal ($\vec{i}_{a_{L\alpha\beta}}$) is

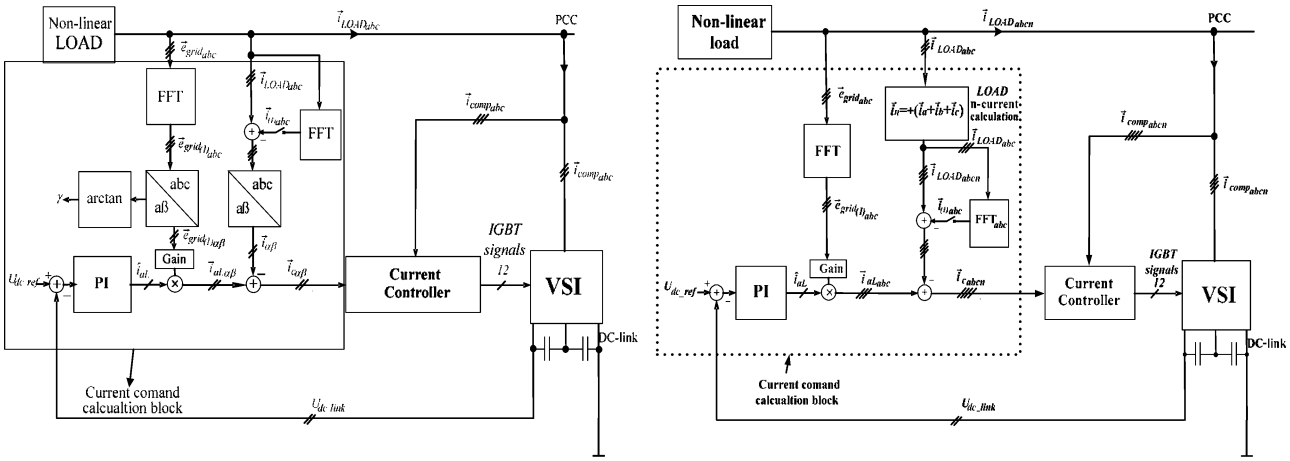

(a) (b)

Fig. 2. Reference current calculation in (a) three-wire systems, and (b) four-wire systems.

added to the reference current in the $\alpha\beta$-coordinates ($\vec{i}_{\alpha\beta}$) to generate the reference compensation current ($\vec{i}_{C_{\alpha\beta}}$), which is the input of the current controller.

In a three-phase four-wire system, due to the presence of the neutral current, the reference current can be calculated, as presented in [10] and [11].

The basic structure of compensation in a four-wire system is shown in Fig. 2(b). The configuration of the controls for the APF in a four-wire system is very similar to that of the three-level VSI shown in Fig. 2(a) except a few components. The dc-voltage controller output signal ($\vec{i}_{aL}$) is added to the reference current of the four-wire system to generate the reference compensation current ($\vec{ic}_{abcn}$), which is the input of the current controller.

The PI controller for the dc-link voltage sets the amplitude of the active current of the APF inverter to regulate the dc-link voltage based on its reference value covering the inverter losses. The amplitude is multiplied by a line-voltage function derived from the line-voltage fundamental vector, which is obtained by the FFT, thus yielding the instantaneous line-current reference. Subtracting the measured load current, the reference value of the APF current is obtained.

The dc-link capacitor will be charged or discharged by the difference of the active load current and grid current, forcing the PI controller to change its output correspondingly, until both active currents are equal. In this way, the APF will compensate all nonactive components of the load current (so-called real-time mode) and regulate the dc-link voltage of the APF.

If cost of the system is of concern, then compensating only load-current harmonics not including the fundamental reactive current will be appropriate. In addition, as an extension of the scheme in [17], the fundamental component of the load current is identified by the FFT algorithm and subtracted from the actual load current fed back (negative) to the summing point behind the multiplier (switch is closed in this case). Then, the fundamental component will not appear in the APF current reference any more (selective mode). Similarly, additional harmonics can be detected by the FFT algorithm and the compensation of these components can be attenuated by an on-demand selective factor. This is advantageous if these harmonics can be regarded as uncritical, not exciting grid resonances. Then, the whole APF-rated power can be applied to the compensation only for the most disturbing or dangerous load current harmonics. The current controller block can be implemented in the stationary *abc*-, $\alpha\beta$-, or rotating *xy*-coordinate system with either a three-wire or a four-wire system and will be explained in the following section.

B. Current Control of the APF With a Three-Level VSI

The configuration of the current control of a three-level VSI-based APF is shown in Fig. 3(a), which is based on a grid-voltage rotating synchronous *xy*-coordinate. The proposed method on the rotating *xy*-coordinates, which is synchronized with the grid voltage, is based on a five-level hysteresis comparator. Five-level hysteresis comparator allows the precise selection of 27 output-voltage space vectors for three-level VSI. It compares the actual phase-current error in the rotating *xy*-coordinates with tolerance bands around the reference current, which are defined as d_x and d_y, as shown in Fig. 3(a), by means of a lookup table implemented in the FPGA. To find the relationship between the *xy*-current error components and the three-level inverter's output-voltage SC U_k represented in the $\alpha\beta$-plane, it is necessary to detect the position of the rotating *xy*-coordinates in relation with the $\alpha\beta$-plane, which is divided into 12 sectors, as shown in [8]. This sector information is delivered to the switching table.

For the sector selection, only the fundamental component of the grid voltage is extracted by FFT for stable and disturbance-free identification.

The transformation angular position γ is calculated as

$$\gamma = \arctan\left(\frac{u_\beta}{u_\alpha}\right). \tag{1}$$

The space-vector position angle γ of the grid voltage obtained from (1) is transformed to a new signal, γ_n, by a lookup table implemented in the FPGA. The digitized variables d_x, d_y and the space-vector position angle of the grid voltage γ_n determine the

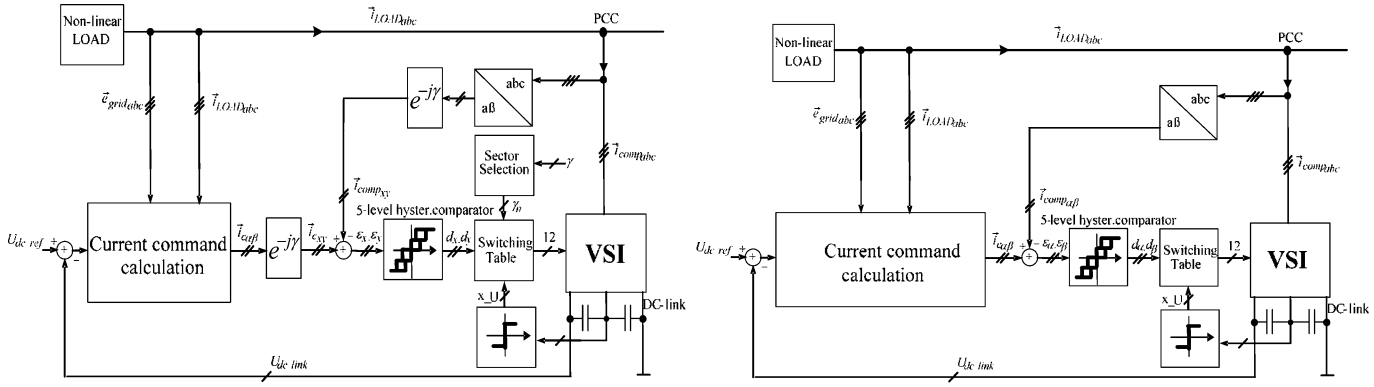

(a) (b)

Fig. 3. Control block diagrams for the three-level VSI-based APF based on (a) the rotating *xy*-coordinates, and (b) stationary $\alpha\beta$-coordinates.

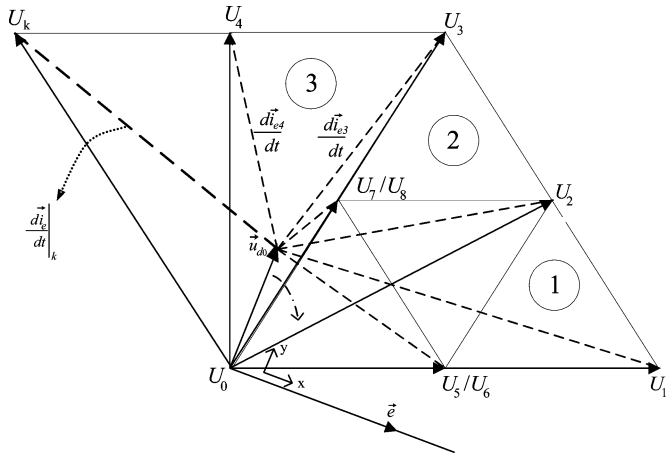

Fig. 4. Derivation of the current error vectors.

addresses of the main lookup table, which is also implemented in the FPGA [9].

The line current error $\vec{i_c}$ is influenced by the output voltage, grid voltage, and derivative of the commanded current. If the current error is zero ($\vec{i_c} = \vec{i}_{\rm comp}$), the desired output voltage vector, $\vec{u}_{do} = s_k \cdot (U_{\rm dc}/2)$, will be defined as

$$\vec{u}_{do} = L\frac{d\vec{i_c}}{dt} + \vec{e}. \tag{2}$$

Otherwise, the desired output voltage vector $\vec{u}_{do}$ will be represented by the space vector $\vec{U}_n$ and the line-current error as follows:

$$L\frac{d\vec{i_e}}{dt} = \vec{u}_{do} - \vec{U}_n. \tag{3}$$

Fig. 4 illustrates an example of proper switching vector selection with the proposed method. The proposed control, which is based on the *xy*-coordinates with the grid vector information (sector 3 for this case), can select switching vectors among $U_1 \sim U_8$. In this case, the length between $\vec{u}_{do}$ and a switching vector is proportional to the amount of the current variation. As an example, the length between U_3 and u_{do} is proportional to $d\vec{i_{e3}}/dt$ as specified in Fig. 4. If the $\vec{u}_{d_0}$ is in sector 3, the proposed control will select inverter-voltage space vectors among U_3, U_4, and U_7/U_8 (U_7 or U_8). However, the conventional methods, without the direct grid voltage information in *xy*-coordinates, would select the voltage vector, U_k in Fig. 4. In addition, the conventional methods, without utilizing the *xy*-coordinates and lacking grid voltage information, can select the voltage vectors, U_2, U_3, and U_4 more frequently than *xy*-coordinates control, as shown in Fig. 5(a). In both cases, $d\vec{i}_{e\,k}/dt$ will be much greater than that of the proposed method. On the other hand, the proposed method utilizes the detected position of the rotating coordinates to estimate the grid voltage vector based on the 12 sectors. The selected switching vectors ($U_{k=}\,(0.27)$ in Fig. 4), with the proposed method, are presented in Fig. 5(b). In this case, the switching vectors causing higher current variation, such as U_2 and U_3, are rarely selected. The simulation results verified the examples of the current error shown in Fig. 4. As a result, current control using the *xy*-coordinates (rotating coordinates) has less current ripple, as shown in Fig. 5(b).

The proposed control integrates the gird-voltage vector to estimate the position of the vector. Based on the position, the control chooses the minimal value of the line-current error $\vec{i_e}$. The proposed control significantly reduces the number of switchings compared with the control in the stationary coordinates as it processes the information about the actual position of the grid-voltage space vector.

The configuration of the controls for an APF on the stationary $\alpha\beta$-coordinates is very similar to that of a three-level VSI shown in Fig. 3(a), except a few components, as shown in Fig. 3(b).

The current control of an APF in a four-wire system is based on the dual-current hysteresis control. The significant advantages of this control are the simplicity and better dynamic response. One disadvantage of the hysteresis control is that there is no limit to the switching frequency, but additional circuitry can be used to limit the maximum switching frequency.

Three-level hysteresis comparators with upper and lower commutation bands are used. The band change can be obtained by a simple logic when two slightly shifted bands are employed. The decision of the commutation band change depends on the phase voltage, e_L, current reference, $i_{\rm ref}$, and line inductance, L_k. Since a three-level VSI is implemented as an APF instead of a two-level VSI, a modification of the conventional three-

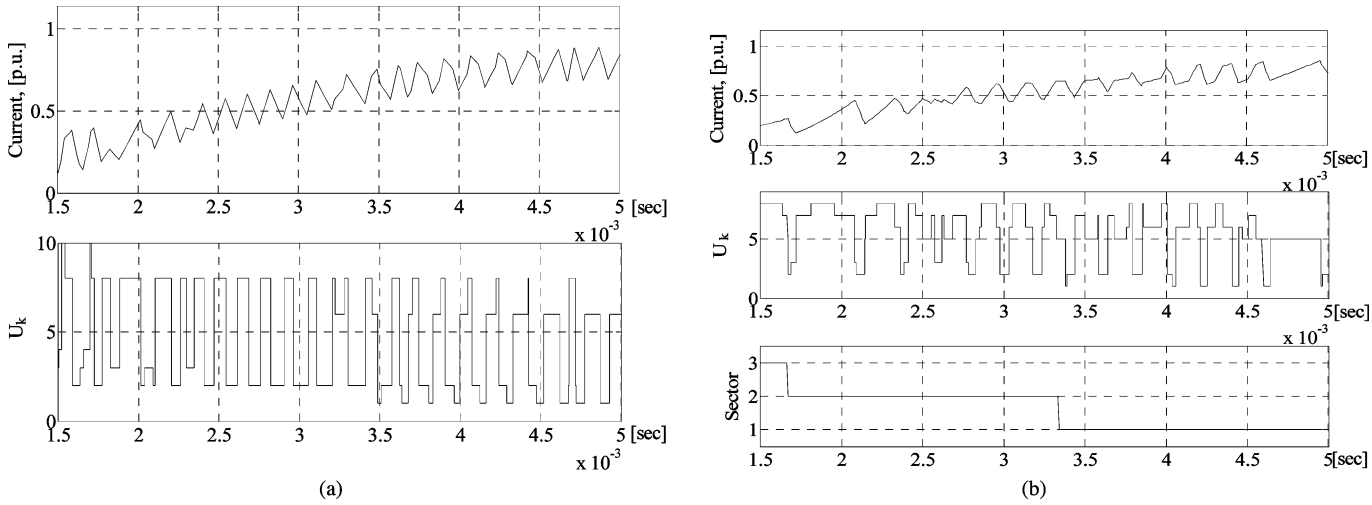

Fig. 5. Switching vector selection example: (a) phase current (top) and space vectors (bottom) using the stationary coordinate control, (b) phase current (top), space vectors (middle), and selected sector (grid-voltage position, bottom) using the proposed control.

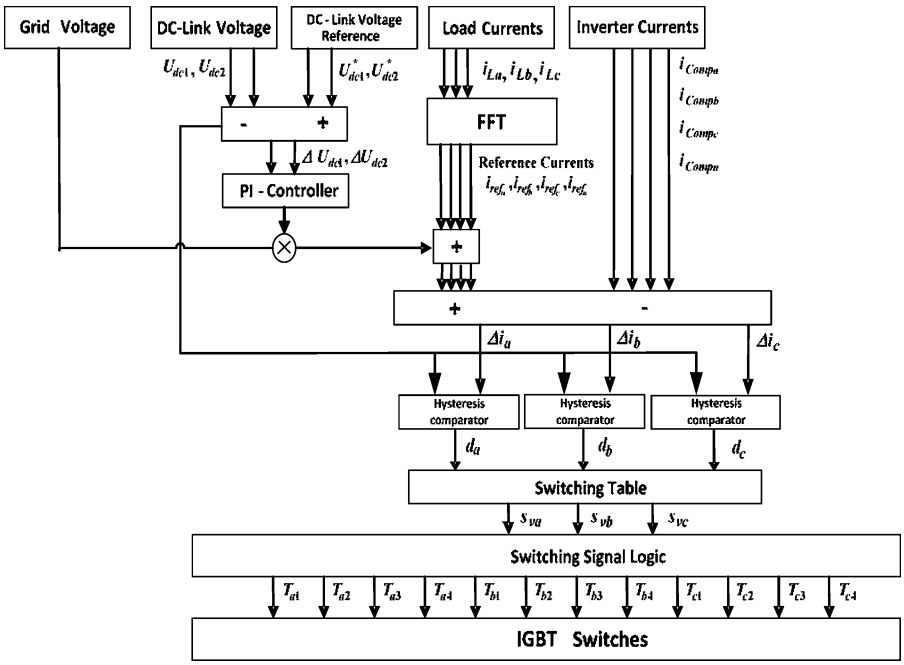

Fig. 6. Control block diagram for the APF in four-wire system.

level hysteresis current controller is required due the neutral-point potential control, as described in [11]. The structure of the three-phase four-wire APF control system is shown in Fig. 6. A traditional proportional–integral (PI) controller is used in order to control the dc-link voltage. The PI controller for the dc-link voltage sets the amplitude of the active current of the APF inverter to regulate the dc-link voltage based on its reference value. The amplitude is multiplied with the line-voltage fundamental component, which is obtained by the FFT, yielding the instantaneous line-current reference. The dc-link neutral-point voltage is controlled by adjusting the hysteresis band positions, with respect to the initial situation. When zero voltage is applied to any phase, the summation of the currents flowing through the clamping diodes, i_{d0}, produces the unbalanced charging of the dc-link capacitors. In this case, a positive current of the i_{d0} charges the dc-link capacitor C_2, and a negative current discharges it. To control the dc-link neutral voltage, the durations of the charging and discharging need to be regulated. Subtracting the measured load current, the reference value of the APF's current is obtained. The current control is based on a three-level hysteresis comparator, comparing the actual phase-current error with tolerance bands around the reference current by means of a lookup switching table implemented in the FPGA. The current controller generates the insulated-gate bipolar transistor (IGBT) firing pulses depending on the sign of dc-link current i_{d0} and the sign of the phase-current error so termed "sign cubical hysteresis

controller" will be appropriate to be used for the implemented control.

C. Design of the LCL-Ripple Filter

The compensation current of an APF usually contains high-frequency components caused by switching actions, which can disturb other EMI-sensitive loads on the common utility grid [18]. Typically, only series inductors are used as a filter, which interface the PWM-inverter and the power grid. In this case, the size of the inductor for optimal switching frequency should be chosen appropriately to reduce the current ripple (harmonics) around the switching frequency [19]. As the inverter ripple current with a hysteresis of 14 A is rather big in comparison to the rated current of 32 A (rms), a second-order line-ripple filter has been inserted between the APF filter and the grid, with grid-side inductors of the same size as those of the filter and capacitive-resistive branches between the lines (Fig. 1). The *LCL*-filters give advantages in costs and dynamic performance since smaller inductors can be used compared to L-filters in order to achieve the necessary damping of the switching harmonics. However, *LCL*-filter design is complex and needs to consider many constraints, such as the current ripple through inductors, total impedance of the filter, resonance phenomenon, reactive power absorbed by filter capacitors, etc. In addition, the *LCL*-filters may cause steady-state and transient distortion in the output current due to resonances. This distortion can be reduced but not solved in PWM converters if the main resonance frequency is selected in a range where no harmonics of the output current exist. With this filter, the switching frequency of the converter has to be high enough to obtain sufficient harmonic attenuation. In the existing controls, this approach cannot be considered since the switching harmonic spectrum is not clearly defined due to the variable switching frequency. This is in contrast to PWM, where the resonance frequency can be chosen easily with frequency lower than the definable lowest pulse frequency, which is roughly twice the switching frequency in the case of a three-level inverter. The *LCL*-filter design in case of PWM will affect the size and cost as shown in *Section III* compared to the existing controls.

To analyze the filtering characteristics in a three-phase three-wire system, one single phase is considered, as shown in Fig. 7. In this case, it should be noted that $C_Y = 3 \cdot C_{\rm filt}$ and $R_Y = 1/3 \cdot R_{\rm filt}$, where $R_{\rm filt}$ and $C_{\rm filt}$ are parameters for each phase. Resistor R_Y, shown in Fig. 7, is utilized to limit the ripple current in order to protect capacitor C_Y.

The transfer function of the *LCL*-filter can be defined as

$$G_{u_{\rm VSI}\to I_{\rm grid}} = \frac{I_{\rm grid}(s)}{U_{\rm VSI}(s)} = -\frac{1}{sL} \cdot \frac{1 + \frac{s}{Q_{\rm filt}\cdot\omega_{\rm filt}}}{1 + \frac{s}{Q_{\rm filt}\cdot\omega_{\rm filt}} + \frac{s^2}{\omega_{\rm filt}^2}}. \quad (4)$$

The resonance frequency $\omega_{\rm filt}$ and quality factor $Q_{\rm filt}$ are given by

$$\omega_{\rm filt} = 2 \cdot \pi f_{\rm filt} = \frac{1}{\sqrt{3 \cdot C_{\rm filt} \cdot \frac{L_{\rm grid}\cdot L_{\rm filt}}{L}}} \quad (5)$$

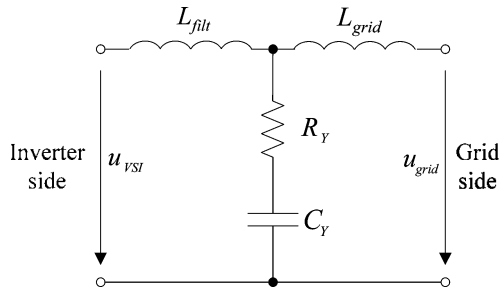

Fig. 7. *LCL*-filter: single-phase case.

$$Q_{\rm filt} = \sqrt{\frac{L_{\rm filt} \cdot L_{\rm grid}}{(L_{\rm filt} + L_{\rm grid}) \cdot C_{\rm filt}}} \cdot \frac{\sqrt{3}}{R_{\rm filt}} \quad (6)$$

where L is the line inductor ($L = L_{\rm filt} + L_{\rm grid} = 2 \cdot L_{\rm filt}$), $U_{\rm vsi}$(s) is the inverter output voltage, and $I_{\rm grid}$ is the grid-side current. $Q_{\rm filt}$ is not high (for the proposed control, $Q_{\rm filt} \approx 1.4$) because of the filter size and costs. LCL-filter gets the maximum attenuation when the inverter-side inductance is equal to the grid-side inductance, as shown in [20]. The frequency responses of the *L*- and *LCL*-filters are shown in Fig. 8.

However, systems incorporating *LCL*-filters are of second order, and there exists a peak amplitude response at the resonant frequency of the *LCL*-filter. This requires more careful design of the *LC*L-filter parameters and current control strategy to maintain system stability since the filters tend to oscillate with the filter resonance frequency.

The most popular method is to insert a damping resistor in the capacitor shunt branch of the LCL-filter, as shown in Fig. 1. The frequency response of the *LCL*-filter with a damping resistor is shown in Fig. 9. As shown in Fig. 9, the damped filter has more attenuation on the resonant frequency, but has less attenuation in the high-frequency region than that of the nondamped filter. In addition, this approach causes considerable power losses.

Fig. 10 shows hysteresis current through the *LCL*-filter resistor. From Fig. 10, the power losses can be calculated as

$$P_L = 3 \cdot R_{\rm filt} \cdot (I_{\rm filt})^2 = 3 \cdot 3.4 \cdot (6.157)^2 = 387\,{\rm W}. \quad (7)$$

Another approach is to actively damp the resonance by control algorithms without increased power losses. The approaches presented in the literature differ in signals used for the control, number of sensors, control complexity, and performance. In [20], an additional feedback of the filter capacitor current is used for damping the resonance to enhance the control performance.

From an industrial point of view, it is desirable to have a minimum number of sensors. Therefore, these approaches are not further considered in this paper since the simulation and experimental results show good performance for the proposed filter, and the cost of the inverter system will not be increased.

An effect of the active damping control loop is the reduction of the harmonic currents that are present in the LCL-filter resonance range. However, the reduction of these harmonic currents

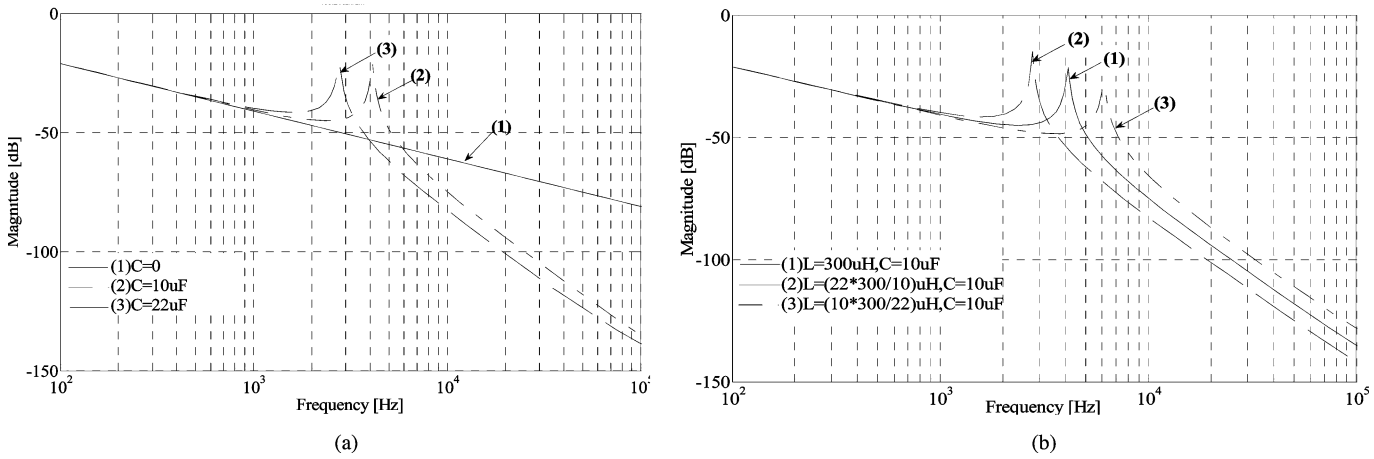

Fig. 8. Transfer functions of an L-filter and an *LCL*-filter with two different filter capacitances. (a) L-filter, (b) *LCL* filter.

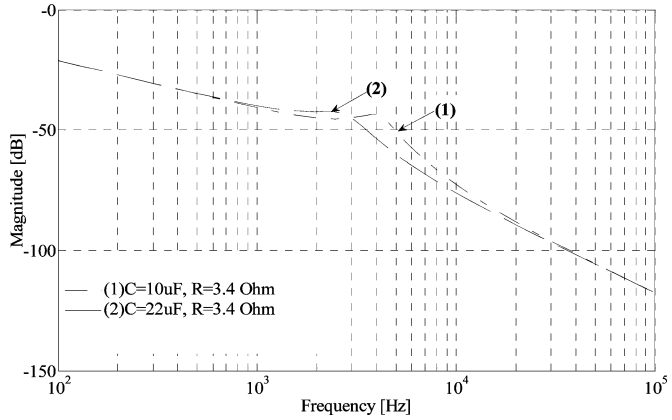

Fig. 9. Transfer functions of an *LCL*-filter with damping resistor and with two different filter capacitances.

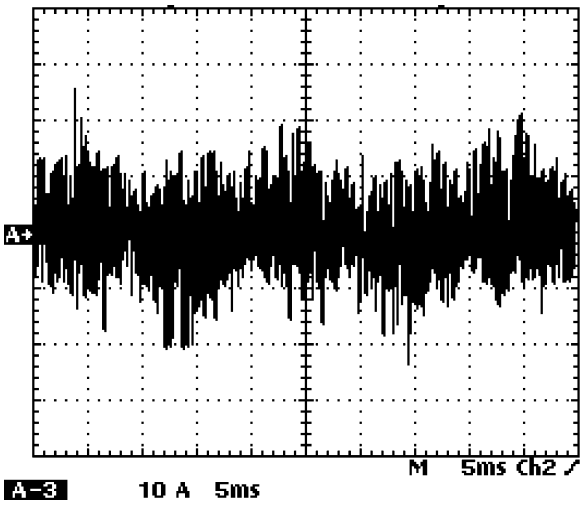

Fig. 10. Current through resistor $R_{\rm filt}$.

causes an increase in the low-order harmonics that are present in the capacitor current, and consequently, results in a reduction in the quality of the output current waveforms. This effect occurs because not only the resonance frequencies are used in the active damping controller, but also all the other harmonics in the capacitor current are included in the active and reactive power references [20].

In addition, an *LCL*-filter is considered and designed for a three-phase four-wire system. The proposed four-wire system *LCL*-filter has a star connection, as shown in Fig. 1(b). In this case, it should be noted that $C_y = C_{\rm filt}$, $R_y = R_{\rm filt}$, and the other filtering characteristics remain the same.

The inherent advantages and drawbacks of the designed *LCL*-filter with different control algorithms are presented and discussed in *Section III.*

III. Simulation Results

Simulation is performed to evaluate and compare the two direct current-space-vector control (DCSVC) control methods in a three-wire system with the same current hysteresis band of $\pm$ 7 A.

The major parameters of the APF system are as follows: dc-link voltage is 700 V, dc-link capacitor size is 4.4 mF, inductor ($L_{\rm filt}$) size is 150 μH, inductor ($L_{\rm grid}$) size is 150 μH, *LCL*-filter capacitor ($C_{\rm filt}$) is 10 μF, *LCL*-filter damping resistor $R_{\rm filt} = 3.4\ \Omega$, and inverter power rating is 30 kVA. Fig. 11 shows the simulated APF system currents with the three-level VSI in a three-wire system based on the control in stationary $\alpha\beta$-coordinates and rotating *xy*-coordinates.

Fig. 12 shows simulation results of the load current of a thyristor bridge with a very large smoothing inductance.

To compare the two controls, a simulation is conducted regarding the total harmonic distortion (THD) and the number of switching times ($W_{dc\Sigma}$) during two cycles with the same hysteresis band. The result is illustrated in Tables I and II, respectively, for the three-level VSI in a three-wire system.

It should be noted that the DCSVC control with an *LCL*-filter caused the switching frequency to increase, as shown in Table II, and as result, a higher power loss and a higher inverter temperature, as shown in *Section IV.*

In addition, the DCSVC method on rotating *xy*-coordinates is compared with a conventional PWM-based control for performance monitoring. The conventional PWM modulator uses two

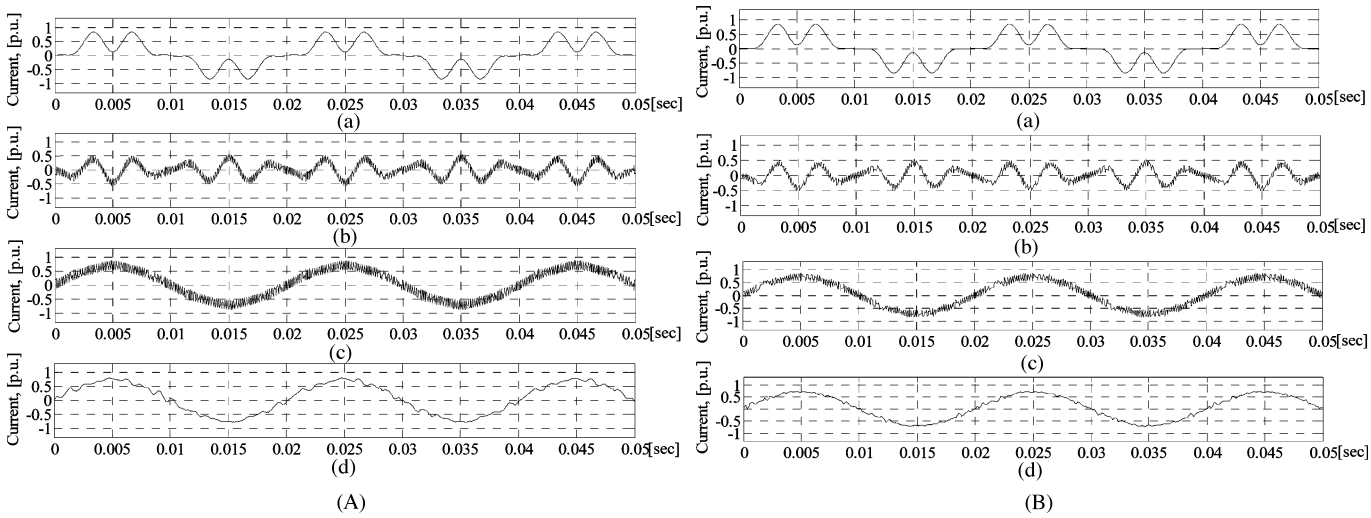

Fig. 11. Simulation results with the three-level VSI (A) based on the control in the stationary $\alpha\beta$-coordinates, and (B) based on the rotating *xy*-coordinates, where (a) load current, (b) compensation current, (c) grid current without ripple filter, and (d) grid current with ripple filter.

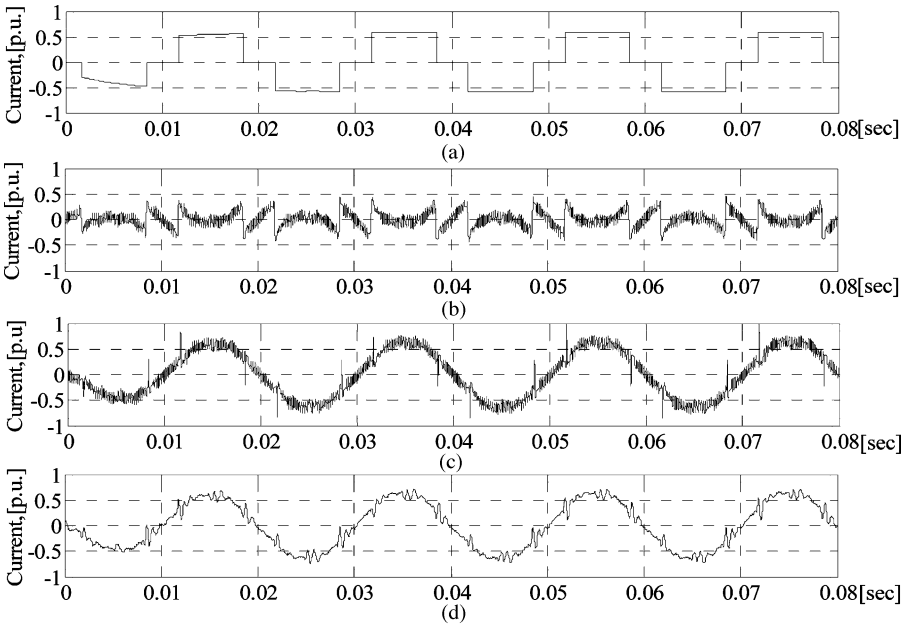

Fig. 12. Simulation results with the three-level VSI based on the control of the rotating *xy*-coordinates with different load: (a) load current, (b) compensation current, (c) grid current without ripple filter, and (d) grid current with ripple filter.

TABLE I
CURRENT HARMONIC SPECTRA DEPENDING ON *LCL*-FILTER PARAMETERS (RELATIVE TO FUNDAMENTAL)

	L_{filt}	L_{grid}	C_{filt}	L_{filt}	L_{grid}	C_{filt}	L_{filt}	L_{grid}	C_{filt}	L_{filt}	L_{grid}	C_{filt}
	150uH	150uH	0uF	50uH	50uH	10uF	150uH	150uH	10uF	250uH	250uH	10uF
Harmonic	$THDi_{,f=20kHz}$=9.68%			$THDi_{,f=20kHz}$=10.46%			$THDi_{,f=20kHz}$=6.25%			$THD_{,f=20kHz}$=9.96%		
5	2.65%			3.94%			2.74%			2.63%		
7	0.81%			1.95%			1.12%			0.91%		
11	2.17%			3.42%			2.21%			2.12%		
13	1,48%			2.72%			1.53%			1.6%		

TABLE II
NUMBER OF SWITCHING DEPENDING ON *LCL*-FILTER PARAMETERS

Control Strategy	L_{filt}	L_{grid}	C_{filt}	L_{filt}	L_{grid}	C_{filt}	L_{filt}	L_{grid}	C_{filt}	L_{filt}	L_{grid}	C_{filt}
	150uH	150uH	0uF	50uH	50uH	10uF	150uH	150uH	10uF	250uH	250uH	10uF
DCSVC,xy	$W_{dc\Sigma}$ = 664 (f_{sw}=5.5kHz)			$W_{dc\Sigma}$ = 1986 (f_{sw}=16.5kHz)			$W_{dc\Sigma}$ = 785 (f_{sw}=6.5kHz)			$W_{dc\Sigma}$ = 687 (f_{sw}=5.7kHz)		
DCSVC,αβ	$W_{dc\Sigma}$ = 1025 (f_{sw}=8.5kHz)			$W_{dc\Sigma}$ = 3094 (f_{sw}=25.8kHz)			$W_{dc\Sigma}$ = 1267 (f_{sw}=10.6kHz)			$W_{dc\Sigma}$ = 1085 (f_{sw}=9.0kHz)		

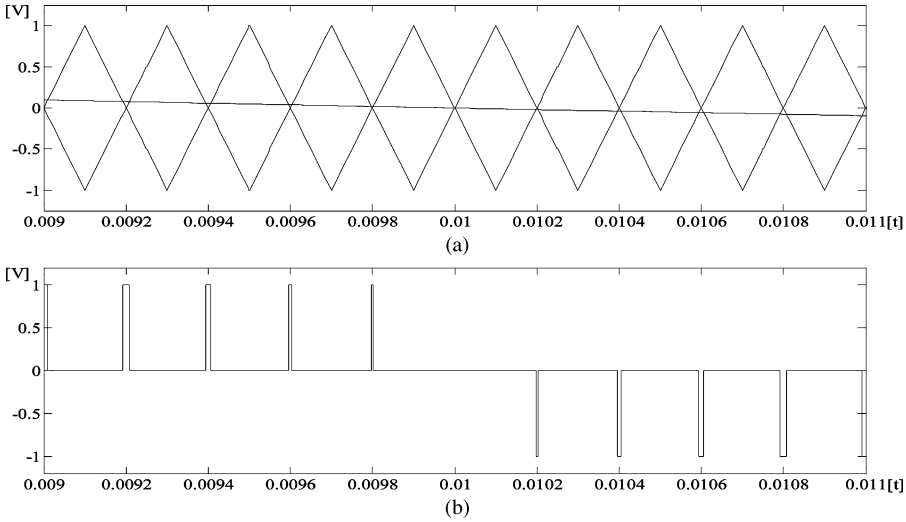

Fig. 13. Three-level PWM strategy. (a) reference signal and triangular carriers, and (b) PWM pulse.

TABLE III
RIPPLE FILTER-SIZE COMPARISON

Control strategy	$THDi_{f=20kHz}$ (total current THD, both controls)	L_{filt}	L_{grid}	C_{filt}
DCSVC	6.25%	150uH	150uH	10uF
PWM	6.08%	210uH	210uH	10uF

symmetrical triangle carriers (double-edge PWM, modulation depth $M = 0.8$), which have opposite phases (one positive and one negative, offset by ± 0.5) as shown in Fig. 13. Each phase reference voltage is compared with each of the triangle carriers. The frequency of the carriers is the switching frequency, and their amplitude is related to the dc-link voltage [9].

For the comparison, control parameters for both methods are adjusted to have almost same THD results. At those conditions, which generate almost same THDs, the total number of switching for both methods is compared in [9]. However, since the proposed method's switching frequency is not fixed like the PWM-based controller, the performance with a line-ripple filter should be evaluated with regard to filter size and THD results. In this paper, the comparison regarding the filter size is presented and shown in Table III.

Since the resonance frequency of the PWM control can be chosen easily with lower frequency than the definable lowest pulse frequency, the size of the *LCL*-filter in case of PWM control is bigger ($L_{\mathrm{filtpwm}} = 1.4 \cdot L_{\mathrm{filtDCSVC}}$), as shown in Table III.

Fig. 14 illustrates the nonlinear load current, compensation current, and grid current using the proposed control strategy on a three-phase four-wire APF. Fig. 15 depicts the neutral load (a), compensation (b), and grid (c) currents.

As shown in Fig. 14, the varying switching frequency in case of the three-level hysteresis current control in a four-wire system complicates the *LCL*-filter design and decreases the performance of the designed *LCL*-filter.

Based on the simulation results, the optimal filter size is selected regarding the costs, switching frequency, and THD, as shown in Table IV. The experimental results are presented in Section IV.

IV. EXPERIMENTAL RESULTS

To validate the performance of the proposed method, a prototype test bed has been built for the 400-V, three-phase utility. Table IV shows the experimental parameters in absolute and per unit values for the three-wire and four-wire systems. For the proposed control, a control board is designed and built. The control board includes voltage and current acquisition circuit and an FPGA. The grid and dc link voltages are measured by VS750B (ABB) transducers and the nonlinear load and inverter currents are measured by ES300C (ABB) transducers. The control board also includes two A/D converters for load current acquisition (LTC-1851, 8-channel, 10 bit, 1.25 MSPS), and for high-frequency inverter current sampling (AD-9201, 2-channel, 10 bit, 20 MSPS). For isolation/protection, fiber optic transmitter (HFBR-1521) and receiver (HFBR-2521) are

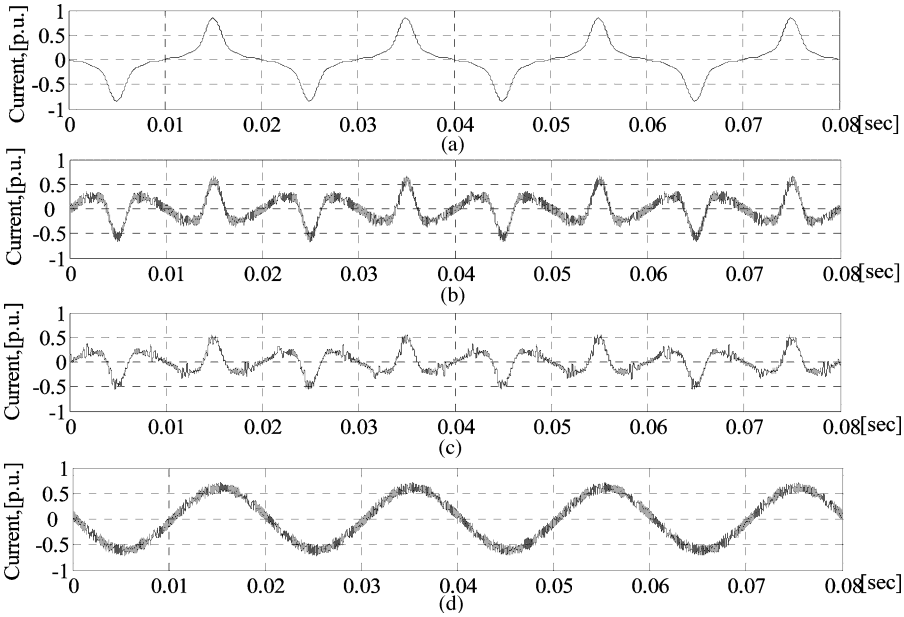

Fig. 14. Simulation results: (a) load current, (b) compensation current without ripple filter, (c) compensation current with ripple filter, and (d) grid current without ripple filter.

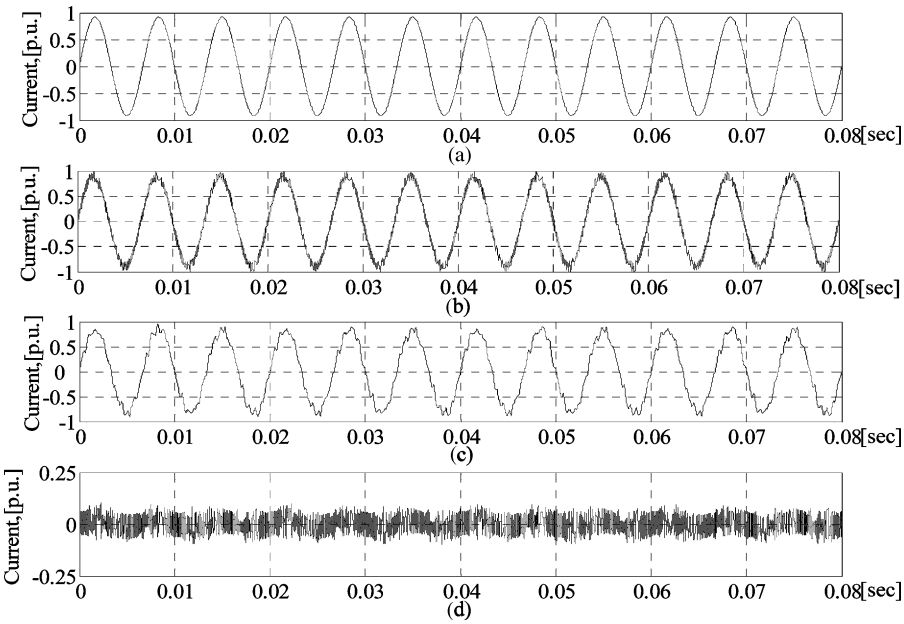

Fig. 15. Simulation results: (a) neutral load current. (b) Neutral compensation current without ripple filter. (c) Neutral compensation current with ripple filter, and (c) Neutral grid current without ripple filter.

TABLE IV
EXPERIMENTAL PARAMETERS

U_{dc}	C_{dc}	S_{inv}	L_{grid}		C_{filt}		R_{filt}		L_{filt}	
700 V	4.4 mF	30 kVA	150μH	0.9%	10 μF	5.01%	3.4Ω	21.3%	150μH	0.9%

used between the control board and the IGBT inverter. The proposed control method is fully implemented in the Xilinx FPGA VIRTEX-II utilizing the Xilinx's integrated software environment (ISE). The FFT algorithm and the coordinate transforms are implemented using the coordinate rotation digital computer (CORDIC) FPGA algorithm [16].

The three-level inverter used in the APF system is designed with IGBT power module (BSM200GB120, Siemens). The measured inverter mean switching frequency is 7.2 kHz. It should be, however, noted that due the proposed control (closed-loop, hysteresis comparators), the switching frequency is not a constant value.

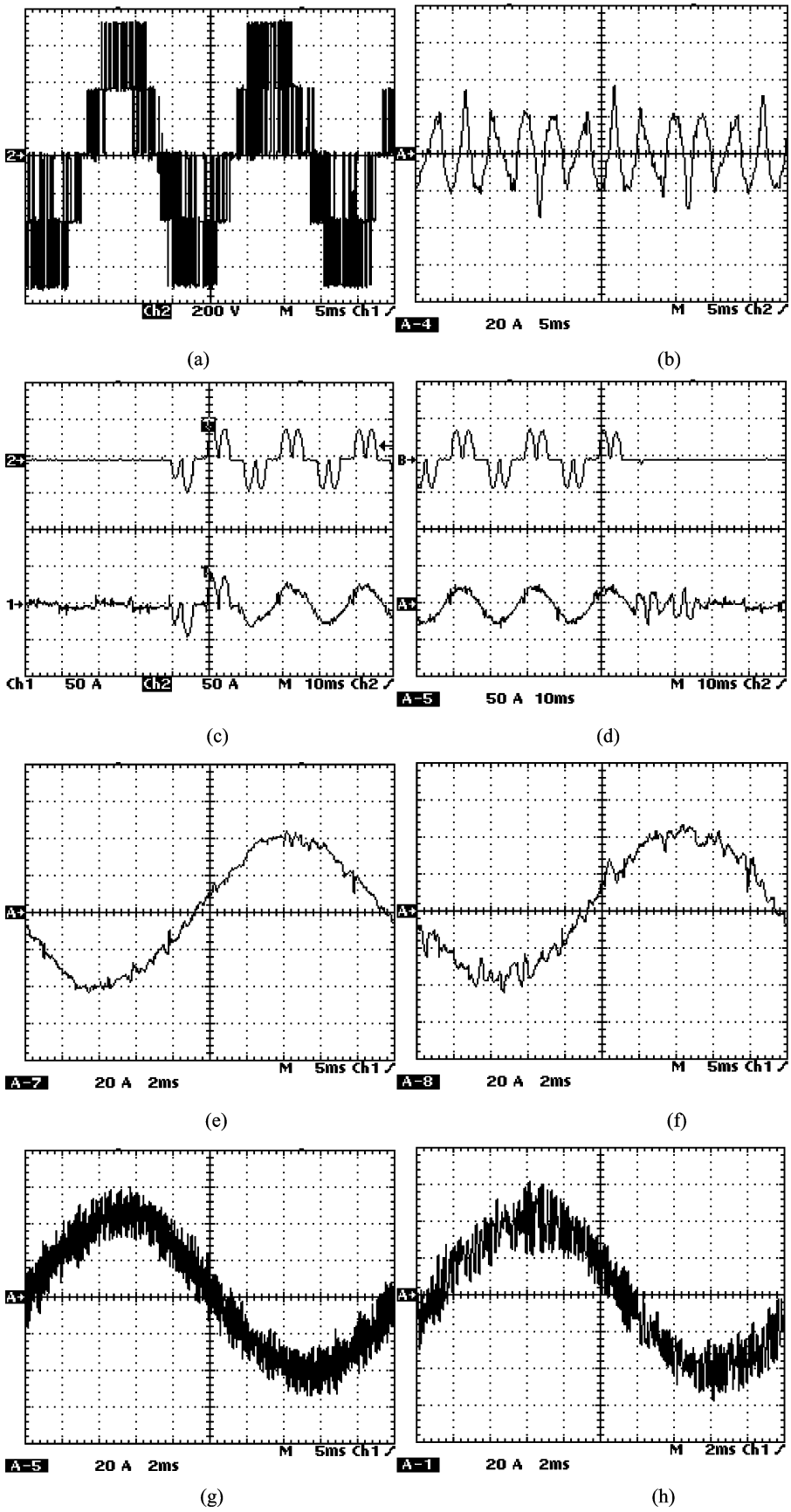

Fig. 16. Experimental results.

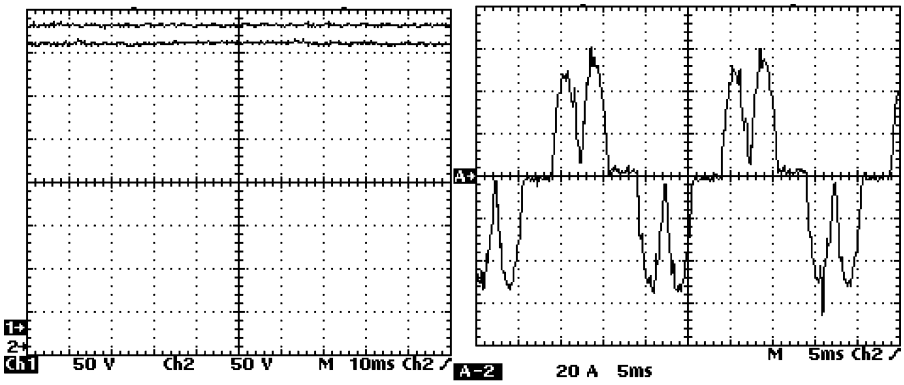

(i) (j)

Fig. 16. *(Continued)* Experimental results.

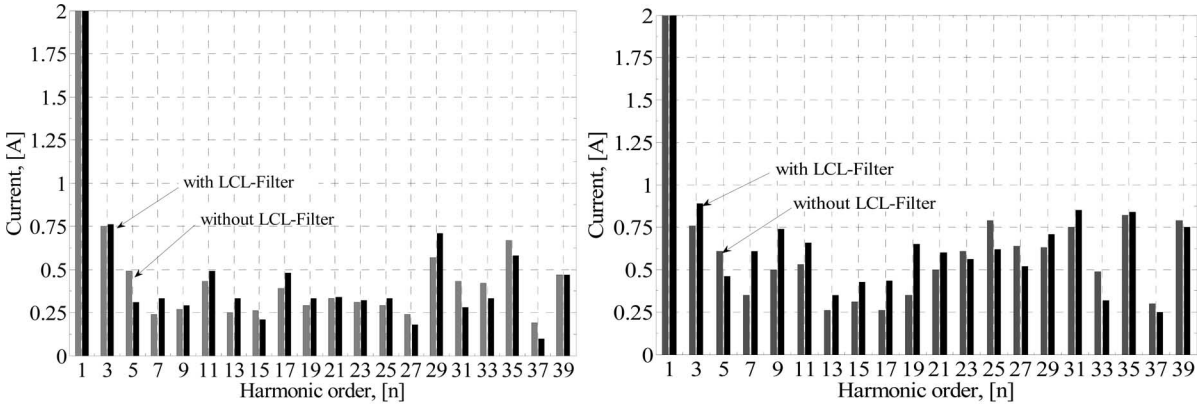

(a) (b)

Fig. 17. Harmonic spectrum comparison: (a) harmonic spectrum of the grid current for the proposed control [Fig. 16 (e) and (g), $THD_{,\,f=2\,\mathrm{kHz}} = 4.4\%$]; (b) harmonic spectrum of the grid current for the controller in the $\alpha\beta$-coordinates [Fig. 16 (f) and (h), $THD_{,\,f=2\,\mathrm{kHz}} = 6.9\%$].

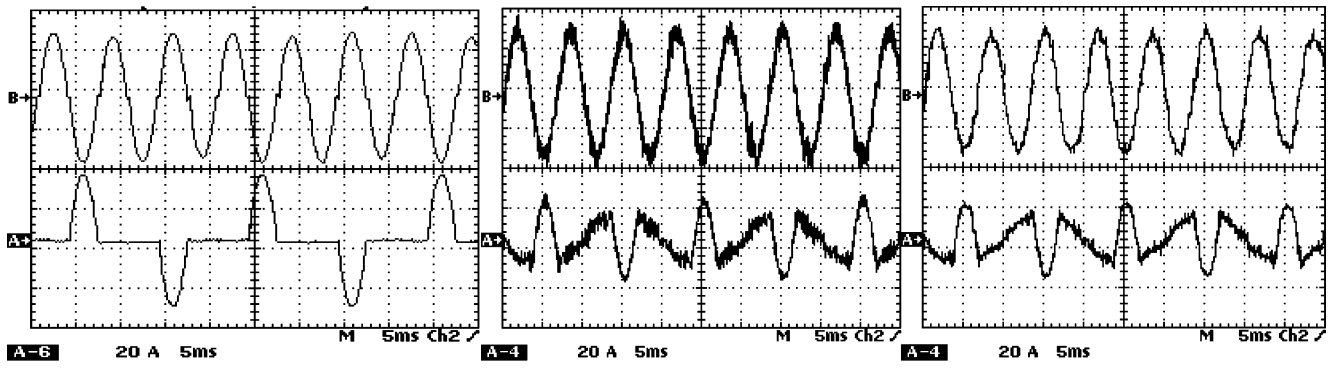

(a) (b) (c)

Fig. 18. Experimental results. (a) Load currents (top) neutral, (bottom) phase a; (b) compensation currents without *LCL*-filter (top) neutral, bottom: phase a; (c) compensation currents with *LCL*-filter (top) neutral, (bottom) phase a.

The load was emulated by a three-phase ac-thyristor controller with a small inductive load, producing similar current waveforms as the three-phase diode rectifier with capacitive smoothing, found very often in industrial drives, but without drawing active power from the grid.

Fig. 16 shows selected experimental results. Fig. 16(a) shows the line-to-line voltage of the three-level inverter with the control in *xy*-coordinates. Fig. 16(b) shows the compensation current in the case where only the harmonic components of the load current are to be compensated. The transient performance of the

proposed control is shown in Fig. 16(c) and (d), by turning ON and OFF the load. The grid current is regulated after an identification period of 20 ms as a sinusoidal waveform. The grid-current waveforms are shown with control in the *xy*-coordinates, as shown in Fig. 16(e) with ripple filter and Fig. 16(g) without ripple filter. The VSI is directly connected to the grid, and the grid impedance being very small, can be neglected. The grid-current waveforms, using control in the $\alpha\beta$-coordinates, with ripple filter and without ripple filter, are shown in Fig. 16(f) and (h) for comparison purpose. Fig. 16(i) shows the well-regulated upper and lower dc-link capacitor voltages. Fig. 16(j) shows the APF current waveforms to compensate both fundamental and harmonic components of the load current (total compensation, real-time mode) with a ripple filter.

Fig. 17 illustrates the comparison of the harmonic content spectrum between the two different control methods. The THD of the inverter output current based on the rotated *xy*-coordinates is lower than that of the control method in the $\alpha\beta$-coordinates. The FFT waveforms are obtained by Tektronix WaveStar software based on one-period (Fig. 16) samples. For a better visualization, y axis is limited at 2A. It should be noted that DCSVC control gained the low-order harmonics in case of *LCL*-filter usage, as shown in Fig. 17. However, the control in the *xy*-coordinates has a better performance and keeps the spectrum in an acceptable level with and without an *LCL*-filter. Another disadvantage of the DCSVC control is the increase of the inverter switching frequency in case of *LCL*-filter usage. The measured inverter temperature with an *LCL*-filter is about 30% higher than the temperature without an *LCL*-filter. One of the solutions for this problem could be a higher inductance for the *LCL*-filter.

The compensation of currents in a four-wire system with and without *LCL*-filter is shown in Fig. 18. It can be seen from Fig. 18(b) that the neutral current is regulated to zero, based on the proposed control. It should be noted that hysteresis controller in a four-wire system decreases the performance of an *LCL*-filter, as shown in Fig. 18(c).

V. Conclusion

In this paper, two DCSVC methods are proposed as a shunt APF based on a three-level voltage-source inverter. Two coordinate systems are studied with one in the *xy*-coordinates rotating synchronously with the fundamental grid-voltage space vector, and the other in the stationary $\alpha\beta$-coordinates. The performance of the inverter system with an *LCL*-filter is analyzed. The DCSVC in the *xy*-coordinates significantly reduces the number of switching with the same current ripple (hysteresis band), compared with a DCSVC in the $\alpha\beta$-coordinates. The APF is able to compensate balanced and unbalanced nonlinear load currents of a four-wire system with the neutral wire connected to the capacitor midpoint. The neutral current of the three-phase four-wire system is regulated and the dc-link neutral-point voltage is balanced under the sign cubical hysteresis controller. The proposed shunt APF can compensate on demand the harmonic currents as well as the reactive currents (full compensation of reactive currents). It adapts itself within one fundamental period to compensate for unexpected variations in the load current, and correct the power factor to near unity in the case of full compensation.

Experiments have been conducted on a 30-kVA test bench with an IGBT-based three-level inverter. The simulation and experimental results validated the performance of the proposed APF control.

References

[1] M. Depenbrock, "A generally applicable tool for analyzing power relations," *IEEE Trans. Power Syst.*, vol. 8, no. 2, pp. 381–387, May 1993.

[2] H. Akagi, "Active harmonic filters," *Proc. IEEE*, vol. 93, no. 12, pp. 315–320, Dec. 2005.

[3] J. Allmeling, "A control structure for fast harmonics compensation in active filters," *IEEE Trans. Power Electron.*, vol. 19, no. 12, pp. 508–514, Mar. 2004.

[4] M. Routimo, M. Salo, and H. Tuusa, "Comparison of voltage-source and current-source shunt active power filters," *IEEE Trans. Power Electron.*, vol. 22, no. 2, pp. 636–643, Mar. 2007.

[5] C. Lascu, L. Asiminoaei, I. Boldea, and F. Blaabjerg, "High performance current controller for selective harmonic compensation in active power filters," *IEEE Trans. Power Electron.*, vol. 22, no. 5, pp. 1826–1835, Sep. 2007.

[6] L. Asiminoaei, P. Rodriguez, and F. Blaabjerg, "Application of discontinuous PWM modulation in active power filters," *IEEE Trans. Power Electron.*, vol. 23, no. 4, pp. 1692–1706, Jul. 2008.

[7] M. Asiminoaei, F. Blaabjerg, and S. Hansen, "Evaluation of harmonic detection methods for active power filter applications," in *Proc. APEC 2005*, vol. 1, pp. 635–641.

[8] O. Vodyakho, D. Hackstein, A. Steimel, and T. Kim, "Novel direct current-space-vector control for shunt active power filters based on three-level inverters," in *Proc. IEEE 23rd Appl. Power Electron. Conf. (APEC 2008)*, pp. 1868–1873.

[9] O. Vodyakho, T. Kim, and S. Kwak, "Comparison of the space vector current controls for active power filters," in *Proc. 2008 IEEE Ind. Electron. Soc. (IECON)*, Orlando, FL, Nov., pp. 612–617.

[10] M. I. M Montero, E. R. Cadaval, and F. B. Gonzalez, "Comparison of control strategies for shunt active power filters in three-phase four-wire systems," *IEEE Trans. Power Electron.*, vol. 22, no. 1, pp. 229–236, Jan. 2007.

[11] O. Vodyakho, T. Kim, and S. Kwak, "Three-level inverter based active power filter for the three-phase, four-wire system," in *Proc. IEEE 39th Power Electron. Spec. Conf. (PESC 2008)*, pp. 1874–1880.

[12] M. E. Ortuzar, R. E. Carmi, J. W. Dixon, and L. Moran, "Voltage-source active power filter based on multilevel converter and ultracapacitor DC link," *IEEE Trans. Ind. Electron.*, vol. 53, no. 2, pp. 477–485, Apr. 2006.

[13] M. P. Kazmierkowski, M. A. Dzienkowski, and W. Sulkowski, "Novel space vector based current controllers for PWM inverters," *IEEE Trans. Power Electron.*, vol. 6, no. 1, pp. 158–166, Jan. 1991.

[14] J. Hurng-Liahng, W. Kuen-Der, W. Jinn-Chang, and C. Wen-Jung, "A three-phase four-wire power filter comprising a three-phase three-wire active power filter and a zig–zag transformer," *IEEE Trans. Power Electron.*, vol. 23, no. 1, pp. 252–259, Jan. 2008.

[15] J. Pou, D. Boroyevich, and R. Pindado, "Effects of imbalances and nonlinear loads on the voltage balance of a neutral-point-clamped inverter," *IEEE Trans. Power. Electron.*, vol. 20, no. 1, pp. 123–131, Jan. 2005.

[16] *Xilinx LogiCore: Fast Fourier Transform v3.2*, 2005, Xilinx, Inc.

[17] J. Ranneberg, "A control of three-level inverter as active power filter with the current control strategy," Ph.D. dissertation, Technische Univ. Berlin, Berlin, 1994.

[18] E. Twining and D. G. Holmes, "Grid current regulation of a three-phase voltage source inverter with an LCL input filter," *IEEE Trans. Power Electron.*, vol. 18, no. 3, pp. 888–895, May 2003.

[19] S. Guoqiao, X. Dehong, C. Luping, and Z. Xuancai, "An improved control strategy for grid-connected voltage source inverters with an LCL filter," *IEEE Trans. Power Electron.*, vol. 23, no. 4, pp. 1899–1906, Jul. 2008.

[20] L. A. Serpa, S. Ponnaluri, P.M. Barbosa, and J. W. Kolar, "A modified direct power control strategy allowing the connection of three-phase inverters to the grid through LCL filters," *IEEE Trans. Ind. Appl.*, vol. 43, no. 45, pp. 1388–1400, Sep./Oct. 2007.

Oleg Vodyakho (S'02–M'07) received the Dr.-Ing. degree in electrical engineering from the University (FernUniversität) of Hagen, Hagen, Germany, in 2007.

From 2002 to 2003, he was a Fellowship Researcher in the Power Electronics Laboratory, University of Applied Science, Konstanz, Germany. He was with Nokian Capacitors, Ltd. as a Research Engineer from 2003 to 2007. He joined the University of Michigan—Dearborn in 2007 as a Postdoctoral Research Associate. His current research interests include power electronics system control, power quality issues, and application and control of inverters and electric drives.

Chris C. Mi (S'00–A'01–M'01–SM'03) received the B.S.E.E. and M.S.E.E. degrees from Northwestern Polytechnical University, Xi'an, China, and the Ph.D degree from the University of Toronto, Toronto, ON, Canada, all in electrical engineering.

He is an Associate Professor of electrical and computer engineering, and Director of DTE Power Electronics Laboratory at the University of Michigan, Dearborn. He is also the Chief Technical Officer of 1Power Solutions, Inc. He was with General Electric Company from 2000 to 2001. He regularly offers a graduate course in electric and hybrid vehicles, and has taught tutorials and led seminars on the subject of hybrid electric vehicles (HEV)/plug-in hybrid electric vehicles (PHEV) for the Society of Automotive Engineers (SAE), the IEEE, the National Science Foundation (NSF), and the National Society of Professional Engineers. He delivered the HEV course to major automotive original equipment manufacturers (OEMs) and suppliers, including GM, Ford, Chrysler, and Delphi. He has offered the tutorial in five countries, including the United States, China, Korea, Malaysia, and Mexico. He has conducted extensive research in EV/HEV space and is the author or coauthor of more than 100 articles. He has delivered keynote speeches at many international conferences.

Dr. Mi became a member of the Eta Kappa Nu, the Electrical and Computer Engineering Honor Society, for being "a leader in education and an example of good moral character." He was the General Chair of the Fifth IEEE International Vehicle Power and Propulsion Conference, Dearborn, MI, September 7–11, 2009. He was the recipient of the 2007 SAE Environmental Excellence in Transportation (E2T) Award for "Innovative Education and Training Program in Electric, Hybrid, and Fuel Cell Vehicles." He is the recipient of the 2005 "Distinguished Teaching Award" of University of Michigan—Dearborn, the IEEE Region 4 "Outstanding Engineer Award," the IEEE Southeastern Michigan Section "Outstanding Professional Award," "the National Innovation Award," and the "Government Special Allowance Award."